Atmos. Chem. Phys., 23, 3937–3953, 2023
https://doi.org/10.5194/acp-23-3937-2023

Atmospheric Chemistry and Physics
Open Access
EGU

Unexpectedly high concentrations of atmospheric mercury species in Lhasa, the largest city in the Tibetan Plateau

Huiming Lin[1], Yindong Tong[2,3], Long Chen[4], Chenghao Yu[5], Zhaohan Chu[1], Qianru Zhang[1], Xiufeng Yin[6], Qianggong Zhang[7,8], Shichang Kang[6,8], Junfeng Liu[1], James Schauer[9,10], Benjamin de Foy[11], and Xuejun Wang[1]

[1]MOE Laboratory of Earth Surface Processes, College of Urban and Environmental Sciences, Peking University, Beijing 100871, China
[2]School of Science, Tibet University, Lhasa 850000, China
[3]School of Environmental Science and Engineering, Tianjin University, Tianjin 300072, China
[4]School of Geographic Sciences, East China Normal University, Shanghai 200241, China
[5]Key Laboratory of Microbial Technology for Industrial Pollution Control of Zhejiang Province, College of Environment, Zhejiang University of Technology, Hangzhou 310014, China
[6]State Key Laboratory of Cryospheric Science, Northwest Institute of Eco-Environment and Resources, Chinese Academy of Sciences, Lanzhou 730000, China
[7]Key Laboratory of Tibetan Environment Changes and Land Surface Processes, Institute of Tibetan Plateau Research, Chinese Academy of Sciences, Beijing 100101, China
[8]CAS Center for Excellence in Tibetan Plateau Earth Sciences, Beijing 100085, China
[9]Department of Civil and Environmental Engineering, University of Wisconsin–Madison, Madison, WI 53718, USA
[10]Wisconsin State Laboratory of Hygiene, University of Wisconsin–Madison, Madison WI 53718, USA
[11]Department of Earth and Atmospheric Sciences, Saint Louis University, St. Louis, MO 63108, USA

Correspondence: Xuejun Wang (wangxuejun@pku.edu.cn) and Yindong Tong (yindongtong@tju.edu.cn)

Received: 1 November 2022 – Discussion started: 7 December 2022
Revised: 27 February 2023 – Accepted: 14 March 2023 – Published: 4 April 2023

Abstract. The city of Lhasa is located in the central Tibetan Plateau and is the most densely populated area. As the first continuous monitoring of atmospheric mercury (Hg) species in a city in the Tibetan Plateau, our monitoring in Lhasa showed that the concentrations of gaseous elemental Hg (GEM), gaseous oxidized Hg (GOM), and particle-bound Hg (PBM) during the subsequent Indian summer monsoon (S-ISM) period were 2.73 ± 1.48 ng m^{-3}, 38.4 ± 62.7 pg m^{-3}, and 59.1 ± 181.0 pg m^{-3}, respectively. During the westerly circulation (WEC) period, the GEM, GOM, and PBM concentrations were 2.11 ± 2.09 ng m^{-3}, 35.8 ± 43.3 pg m^{-3}, and 52.9 ± 90.1 pg m^{-3}, respectively. The GOM and PBM concentrations were higher than those of previous monitoring in the Tibetan Plateau and other provincial capitals in China. Typical high-value occurrence processes were studied to investigate random events with high atmospheric Hg concentrations in Lhasa. Combustion events nearby or further away may be the main contributor of the high-concentration events. The lowest GEM concentrations occurred in the afternoon, and persistently high concentrations were observed at night. The changes in GEM concentrations were consistent with the trends of other pollutant concentrations and contradictory to those of the wind speed. The high GEM concentrations at night can be attributed to the lower boundary layer height and lower wind speed. For both GOM and PBM, higher GOM concentrations occurred during the day and PBM during the night. The results of the principal component analysis indicated that local sources and wind speed are important factors influencing atmospheric Hg concentrations in Lhasa. The trajectory simulation showed that the source of the GEM in Lhasa gradually shifted from the south to the west of Lhasa from the S-ISM to the

WEC periods, while both the southern and western sources were important in the late WEC period. The concentrations and change patterns of Hg species in Lhasa were significantly different than those at other monitoring sites in the Tibetan Plateau. Monitoring Hg species in Lhasa shows the possible maximum anthropogenic influences in the Tibetan Plateau and demonstrates the dramatic effect of wind on changes in urban atmospheric Hg concentrations.

1 Introduction

Mercury (Hg) has received worldwide attention owing to its high toxicity and bioaccumulation. Atmospheric mercury (Hg) exists in three different forms: atmospheric gaseous elemental Hg (GEM), gaseous oxidized Hg (GOM), and particle-bound Hg (PBM) (Selin, 2009). They exhibit different behaviors in the environment owing to their various chemical properties (Selin, 2009; Travnikov et al., 2017; Lindberg and Stratton, 1998; Seigneur et al., 2006). Many established monitoring networks for atmospheric Hg exist in North America and Europe (Stylo et al., 2016) including the Atmospheric Mercury Network (AMNet; Gay et al., 2013), the Global Mercury Observation System (GMOS; Sprovieri et al., 2013, 2016), the Canadian Atmospheric Mercury Network (CAMNet; Kellerhals et al., 2003), and the Arctic Monitoring Assessment Programme (AMAP; https://mercury.amap.no/, last access: 30 March 2023) (Gay et al., 2013; Sprovieri et al., 2013, 2016; Kellerhals et al., 2003). They have been operating for decades and have provided a large amount of atmospheric Hg data. Compared to Europe and the United States, independent research teams have conducted monitoring work in China based on different research interests (X. Fu et al., 2012, 2008, 2016, 2019; Liu et al., 2011; Feng et al., 2013; Wang et al., 2015; Hu et al., 2014; Ci et al., 2011; Duan et al., 2017; Liu et al., 2002; Yin et al., 2018, 2020; Lin et al., 2022, 2019). Most monitoring stations are set up only in developed regions, such as eastern and central China, owing to operational difficulties in remote areas. Few studies on atmospheric Hg in western China have been reported; thus, little is known about the overall level of atmospheric Hg in western China. To better employ the Minamata Convention and verify the effect of the implementation of the convention, monitoring atmospheric Hg concentrations around the globe is significant and can aid in identifying the global Hg transport pattern.

The Tibetan Plateau is in the midlatitudes of the Northern Hemisphere (in central Asia) and is an important area for studying the global Hg circulation. Owing to the high altitude and rough living conditions, there is little Hg research on the Tibetan Plateau. This area is less developed, and there are few industrial activities; therefore, it is generally considered a clean region and can be treated as a background condition. However, there are large tourist cities in this area, such as Lhasa, where the number of tourists reached 40 121 522 in 2019 (Tibet Bureau of Statistics, 2020). Local cement production in Tibet reached 10.81×10^6 t in 2019 (Tibet Bureau of Statistics, 2020). Meanwhile, although the high altitude makes the Tibetan region a natural barrier between inland China and the Indian subcontinent (Qiu, 2008; Yao et al., 2012; Pant et al., 2018), the Tibetan Plateau is potentially influenced by the Indian summer monsoon (ISM) and the westerly circulation (WEC). Transboundary inputs of atmospheric pollutants to the Tibetan Plateau have been demonstrated in pollutant studies such as with persistent organic pollutants and black carbon (Yang et al., 2018; Li et al., 2016b; R. Zhang et al., 2015; Pokhrel et al., 2016; Wang et al., 2018; Feng et al., 2019; Zhu et al., 2019). Our previous study on atmospheric Hg in the Qomolangma National Nature Preserve (QNNP) region also suggested that atmospheric Hg from India can be transported and affect atmospheric Hg concentrations in the Tibetan Plateau as a result of the Indian monsoon (Lin et al., 2019). Hence, it remains unclear whether the Tibetan Plateau can be treated as a background area for studying atmospheric Hg, and further monitoring data are required. Monitoring in the largest cities in the Tibetan Plateau will provide important information and corroboration to address this query.

In a previous study, Yin et al. (2018) reported GEM concentration data for the Namco region in the Tibetan Plateau from 2012–2014 and found that the GEM concentration at Namco was $1.33 \pm 0.24\,\mathrm{ng\,m^{-3}}$, which is lower than the mean GEM concentration in the Northern Hemisphere (Lindberg et al., 2007; Slemr et al., 2015; Venter et al., 2015; Sprovieri et al., 2016; Lan et al., 2012). Our previous study at the QNNP (Lin et al., 2019) showed that the atmospheric Hg concentrations were $1.42 \pm 0.37\,\mathrm{ng\,m^{-3}}$, $21.4 \pm 13.4\,\mathrm{pg\,m^{-3}}$, and $25.6 \pm 19.1\,\mathrm{pg\,m^{-3}}$ for GEM, GOM, and PBM, respectively, which is quite similar to the average GEM concentrations in the Northern Hemisphere (Lindberg et al., 2007; Slemr et al., 2015; Venter et al., 2015; Sprovieri et al., 2016; Lan et al., 2012). The concentrations of atmospheric Hg species in Nyingchi, in the southeast Tibetan Plateau, were very low ($1.01 \pm 0.27\,\mathrm{ng\,m^{-3}}$, $12.8 \pm 13.3\,\mathrm{pg\,m^{-3}}$, and $9.3 \pm 5.9\,\mathrm{pg\,m^{-3}}$ for GEM, GOM, and PBM, respectively), which may be affected by heavy wet deposition and the large amounts of vegetation in the Yarlung Zangbo–Brahmaputra Canyon (Lin et al., 2022). However, Namco, the QNNP, and Nyingchi are remote areas in the plateau, with a low population and little industry. During previous studies in Lhasa, the largest city in the plateau, only dry and wet depositions of at-

mospheric Hg were analyzed. Monitoring of atmospheric Hg particulate matter (Huang et al., 2016a) indicated that Lhasa has mean particulate Hg levels as high as 224 pg m^{-3} (ranging from 61.2 to 831 pg m^{-3}), which is much higher than expected. Huang et al. (2013) measured the wet deposition of atmospheric Hg in Lhasa in 2010 and showed that the wet depositions of total Hg concentration and particulate Hg concentration were higher during the non-monsoon period than those during the monsoon period. The active Hg was higher during the monsoon than during the non-monsoon period, and they concluded that the wet deposition of Hg originated mainly from local sources. This indicates that atmospheric Hg concentrations in Lhasa may be elevated, and further detailed monitoring is needed.

In this study, we conducted a high-time-precision atmospheric Hg species monitoring system in Lhasa. We performed continuous measurements of GEM, GOM, and PBM concentrations from the subsequent Indian summer monsoon (S-ISM) period to the WEC period from 2016 to 2017. Based on literature research, this is the first continuous monitoring of atmospheric Hg species in a city in the Tibetan Plateau, and the influence of human activities, meteorological factors, and long-range transportation of pollutants on the diurnal variation of atmospheric Hg in Lhasa is discussed. We combined monitoring with other pollutant concentrations to explore the main factors influencing the local atmospheric Hg concentrations. To determine the detailed source profile of atmospheric Hg, we combined real-time Hg monitoring data with backward trajectory and cluster analyses. This study can help understand atmospheric Hg characteristics in the city of the plateau and provide scientific support for managerial decision-making.

2 Material and methods

2.1 Atmospheric Hg monitoring sites

The monitoring site for atmospheric Hg species in Lhasa was set up on the top floor of the Lhasa station office building in the Institute of Tibetan Plateau Research, Chinese Academy of Sciences, in the west of the city of Lhasa (29.64° N, 91.03° E; 3650 m a.s.l., above sea level; Figs. 1 and S1 in the Supplement). The monitoring in Lhasa included the subsequent Indian summer monsoon (S-ISM; 29 August to 30 September 2016) and westerly circulation (WEC; 1 October 2016 to 2 February 2017) periods from 29 August 2016 to 2 February 2017. To better understand the changes of atmospheric Hg concentrations in different periods, the WEC period was further divided into WEC1 (1 October to 30 December 2016) and WEC2 (1 January to 2 February 2017) periods. Lhasa is located in the central region and is the largest city in the Tibetan Plateau, covering an area of approximately 60 km^2. The Lhasa population in 2019 was 720 700, accounting for approximately 20.6 % of the total population of the Tibet Autonomous Region (Tibet Bureau of Statistics, 2020). The entire city is in a flat river valley surrounded by mountains of up to 5500 m a.s.l. During the ISM period (from May to September), the low pressure in the Tibetan Plateau attracts the summer monsoon from the Indian Ocean to the plateau, exhibiting a wetter monsoon season (Qiu, 2008). During the non-monsoon season (from October to April), the large-scale atmospheric circulation in the Tibetan Plateau is mainly under the control of westerly winds, which largely come from the inland areas of central Asia, presenting a drier season in Lhasa during this time (Huang et al., 2010; Guo et al., 2015). According to previous studies, the air quality in Lhasa may be influenced by local emissions from anthropogenic activities (e.g., power plants, cement facilities, vehicular traffic, and religious activities) (Li et al., 2008; Cong et al., 2011; Huang et al., 2010; Guo et al., 2015; Wang et al., 2016; Li et al., 2016a) and long-range transboundary atmospheric transport (Huang et al., 2016a, b).

2.2 GEM, GOM, and PBM active monitoring

Monitoring in Lhasa was performed using Tekran models 2537 B, 1130, and 1135 (Tekran Inc., Toronto, Canada) for real-time continuous measurements of GEM, GOM, and PBM concentrations. Model 2357b is the main analytical module used to analyze Hg concentrations employing the cold atomic fluorescence technique. Model 1130 is divided into pump and lysimeter modules and mainly used for the collection and resolution of GOM. Model 1135 is the particle collection module that is mainly used to collect and analyze atmospheric Hg in the particulate state. During the actual monitoring, considering the low air pressure in the Tibetan Plateau, we reduced the airflow of the pump module to 7.5 L min^{-1} (Swartzendruber et al., 2009; H. Zhang et al., 2015, 2016; Lin et al., 2019, 2022), and the airflow in model 2537B was reduced to 1 L min^{-1} to ensure that atmospheric Hg monitoring could be continuously performed. All monitoring data were converted to concentrations under standard atmospheric pressure. The Tekran 2537B analyzer was automatically calibrated every 23 h using the instrument's internal Hg permeation source and was calibrated before and after monitoring using an external Hg source. The same instrument setup was used for the QNNP and Nyingchi (Lin et al., 2019, 2022). The Tekran ambient Hg analyzer has been described in detail in previous studies (Landis et al., 2002; Rutter et al., 2008; de Foy et al., 2016).

2.3 Meteorological data and other pollutant data

During the monitoring period, the Vantage Pro2 weather station (Davis Instruments, USA) recorded local temperature (accuracy of 0.1 °C), relative humidity (accuracy of 1 %), wind speed (accuracy of 0.1 m s^{-1}), wind direction (accuracy of 1°), barometric pressure (accuracy of 0.1 hPa), solar radiation (accuracy of 1 W m^{-2}), and UV index (accuracy 0.1 MEDs). Hourly measurements of $PM_{2.5}$, PM_{10}, SO_2,

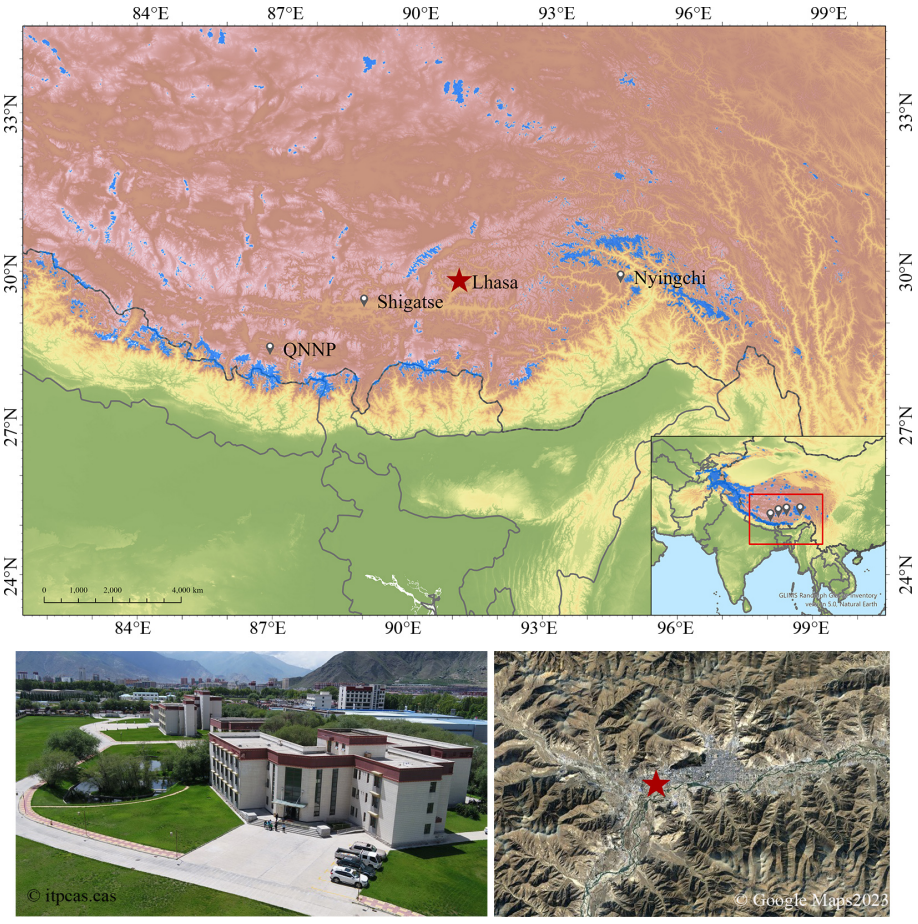

Figure 1. Location of the Lhasa station in the Institute of Tibetan Plateau Research, Chinese Academy of Sciences (red star).

NO_2, O_3, and CO concentrations and the air quality index (AQI) were obtained from monitoring stations hosted by the Ministry of Ecology and Environment of China and published by the China Environmental Monitoring Center. The station was set up 10 km from the atmospheric Hg monitoring station.

2.4 Backward trajectory simulation and potential source analysis

To better understand the transport paths of atmospheric GEM, the Hybrid Single-Particle Lagrangian Integrated Trajectory (HYSPLIT) model was used to calculate backward trajectories (Stein et al., 2015; Chai et al., 2017, 2018; Hurst and Davis, 2017; Lin et al., 2019). The HYSPLIT model (https://www.arl.noaa.gov/hysplit/hysplit/, last access: 30 March 2023) is a hybrid approach that combines Lagrangian and Eulerian methods, which was developed by the National Oceanic and Atmospheric Administration (NOAA) as a tool to explain the transport, dispersion, and deposition of particles in the atmosphere. The backward trajectory simulation used Global Data Assimilation System (GDAS) data with $1° \times 1°$ latitude and longitude horizontal spatial resolution and 23 vertical heights every 6 h in this study. We examined the effect of arrival height on the trajectories using different arrival heights (50, 100, 400, and 1000 m) in December 2016 (Fig. S2). The results showed that the calculated trajectories of the air masses were almost the same when the arrival height was below 400 m. The trajectory arrival altitude was then set to 100 m a.g.l. in this study. The trajectories were computed every 6 h with an inverse time of 120 h. The trajectories could cover China, Nepal, India, Pakistan, and most of west Asia. Here, we combined the backward trajectory with real-time Hg monitoring concentrations to represent the trajectories of GEM concentrations. Cluster analysis was performed after the trajectory calculation. Cluster analysis can indicate the main trajectory of incoming pathways and the GEM concentration indicated by the incoming trajectories.

2.5 Principal component analysis

Principal component analysis (PCA) is a data reduction method that allows a number of measured variables to be cat-

egorized into several factors that represent the behavior of the entire dataset (Jackson, 2005). In many previous Hg studies, PCA has been used to analyze the relationships between Hg and multiple pollutants and meteorological variables (Brooks et al., 2010; Cheng et al., 2012; Liu et al., 2007; Zhou et al., 2019; Lin et al., 2022). Prior to running the PCA, all variables were normalized by the standard deviation. To check whether PCA was the appropriate method for the dataset used in this study, Kaiser–Meyer–Olkin's measure of sampling adequacy (MSA > 0.5) and Bartlett's test of sphericity ($P < 0.05$) tests were performed during data analysis. Total variance and rotated scree plots were used to determine the number of factors during the PCA, and components with variance ≥ 1.0 were retained. Variables with high factor loadings (generally > 0.5) were identified as potential sources of Hg in this study.

3 Results and discussion

3.1 Atmospheric Hg monitoring in Lhasa

Atmospheric Hg monitoring in Lhasa comprised the subsequent Indian summer monsoon (S-ISM) and westerly circulation (WEC) periods from 29 August 2016 to 2 February 2017. Figure 2 shows the variation in atmospheric Hg concentrations at the station during the monitoring period. During the whole monitoring period, the mean concentrations of GEM, GOM, and PBM at the station were $2.26 \pm 1.97\,\mathrm{ng\,m^{-3}}$, $36.4 \pm 48.9\,\mathrm{pg\,m^{-3}}$, and $54.5 \pm 119.5\,\mathrm{pg\,m^{-3}}$ (mean concentration $\pm$ standard deviation), respectively. During the S-ISM period, the concentrations of GEM, GOM, and PBM were $2.73 \pm 1.48\,\mathrm{ng\,m^{-3}}$, $38.4 \pm 62.7\,\mathrm{pg\,m^{-3}}$, and $59.1 \pm 181.0\,\mathrm{pg\,m^{-3}}$, respectively. While during the WEC period, the concentrations of GEM, GOM, and PBM were $2.11 \pm 2.09\,\mathrm{ng\,m^{-3}}$, $35.8 \pm 43.3\,\mathrm{pg\,m^{-3}}$, and $52.9 \pm 90.1\,\mathrm{pg\,m^{-3}}$, respectively. The GEM concentrations during the S-ISM period were significantly higher than those during the WEC period ($p < 0.01$), while the mean concentrations of GOM and PBM in the S-ISM period were slightly higher than those in the WEC period. Overall, GEM concentrations showed a decreasing trend throughout the monitoring period, with the average weekly concentration decreasing from $3.21\,\mathrm{ng\,m^{-3}}$ at the beginning of the monitoring period to $1.60\,\mathrm{ng\,m^{-3}}$ at the end of the monitoring period, which is in contrast to previous studies, which showed that atmospheric Hg concentrations in the Northern Hemisphere are low in summer and high in winter (Horowitz et al., 2017; Jiskra et al., 2018). The different variation trends between Lhasa and the whole Northern Hemisphere may be related to the special location of Lhasa. Unexpectedly high concentrations were found at irregular intervals for all Hg species. The occurrence time of these high concentrations was random, and high GEM concentrations did not always occur at the same time as high GOM or PBM concentrations, indicating the complexity of the Hg sources of the species. For GOM and PBM, relatively comparable trends between them may be related to similar sources, transport, and transformation reactions in the atmosphere.

In early September, GOM concentrations were generally higher than PBM concentrations. In the subsequent period, PBM concentrations were always higher than GOM concentrations, which may indicate that the sources and composition of pollutants at this time were not consistent with those in the latter period. GOM and PBM may undergo mutual transformation in the atmosphere, which may be related to temperature, humidity, and atmospheric composition (Rutter and Schauer, 2007; Rutter et al., 2008), and thus the concentration distributions of GOM and PBM may also be related to the changes of local climate and atmospheric composition from S-ISM to WEC periods. The GOM and PBM concentrations were higher in November and December. Since GOM and PBM are mainly from local emissions, the changes in their concentrations may indicate that there are more local sources in this period. As Lhasa enters the heating season in November–December, and there are more local religious activities at this time, there may be more local combustion sources. Table 1 lists the concentrations of Hg and other pollutants during the monitoring period. $PM_{2.5}$ concentration increased significantly in the WEC1 period, indicating the presence of more particulate matter during this period. This could explain the elevated concentrations of GOM and PBM from November–December.

Table 2 shows the distributions of atmospheric Hg concentrations in some provincial capitals in China and nearby monitoring stations from literature. In general, the GEM concentration in Lhasa is low among the provincial capitals in China. The GEM concentration in other provincial capitals of China was approximately $3–10\,\mathrm{ng\,m^{-3}}$. Guiyang, Chongqing, and Lanzhou were the nearest provincial capitals to Lhasa, with GEM concentrations reported in the literature, all located in western China. Guiyang had a very high GEM concentration due to the presence of local Hg mines (Liu et al., 2011). The GEM concentration in Chongqing was approximately 3 times higher than that of Lhasa. The higher GEM concentration in Chongqing was likely due to its proximity to the Hg-contaminated area and large population (Yang et al., 2009). Compared to Lanzhou, another high-altitude city, the GEM concentration in Lhasa was approximately half that of Lanzhou, which may be owing to the overall cleaner environment with fewer local pollution sources in Lhasa (Yin et al., 2020). The GOM and PBM concentrations in other provincial capitals were relatively less monitored. However, GOM concentrations in Lhasa were significantly higher than those in cities with GOM monitoring, such as megacities like Beijing and Shanghai, and even higher than those in Guiyang, where Hg mines are located. GOM concentrations in provincial capitals nationwide were mainly concentrated between $3–20\,\mathrm{pg\,m^{-3}}$, whereas the GOM concentrations in Lhasa were approximately 2–10 times higher

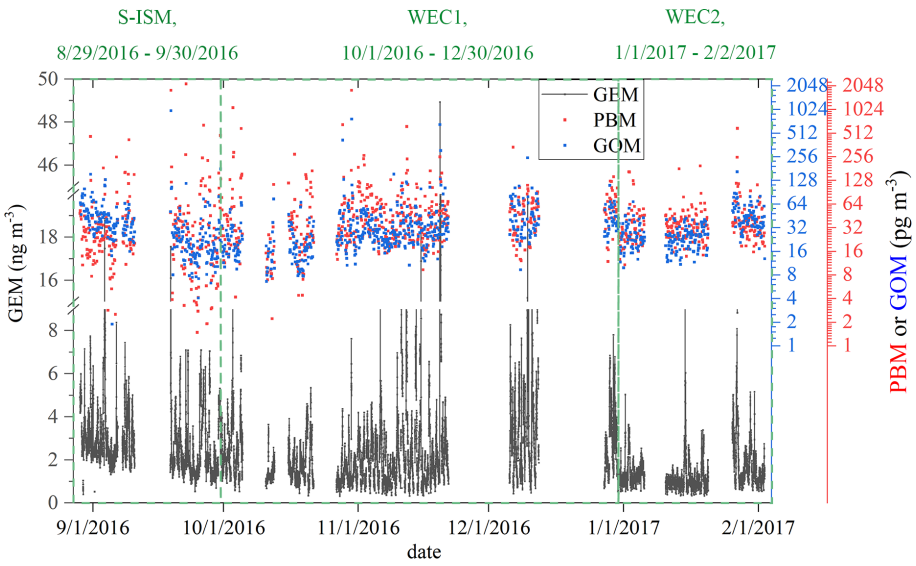

Figure 2. Time series of GEM, GOM, and PBM concentrations over the sampling period. The GEM concentration resolution was 5 min, and the GOM and PBM resolutions was 2 h.

than the average concentration in provincial capitals. The high GOM concentration in Lhasa is likely due to its high altitude. Lhasa is exposed to much higher solar radiation and has more ice surfaces than inland areas, which may have contributed to the oxidation of GEM or the re-release of GOM deposited in snow and ice (Steffen et al., 2008; Dommergue et al., 2003; Song et al., 2018). In contrast, the PBM concentration in Lhasa was at a lower level, only somewhat higher than that in Hefei. The monitoring period in Lhasa was mainly in winter when there were more particulate matter emissions than in summer owing to heating combustion. The $PM_{2.5}$ concentration in Lhasa was low throughout the monitoring period (Table 1), which indicated that the local particulate matter emissions were low; this may be the main reason for the low PBM concentration.

Compared to nearby monitoring stations (Table 2), Hg species concentrations in Lhasa were high. Namco station is the nearest station; its altitude is 4730 m, and the distance between the two stations is approximately 120 km. The GEM concentration in Namco was 1.33 ± 0.24 ng m^{-3}, which was only 59 % of Lhasa. This is likely because the Namco region is sparsely populated with minimal local pollution and is far from major Hg pollution sources (Yin et al., 2018). Compared to the QNNP (Lin et al., 2019) on Mt. Everest, which is approximately 500 km away, the GEM, GOM, and PBM concentrations in Lhasa were approximately 1.6, 1.7, and 2.1 times higher, respectively. Our previous studies demonstrated that the QNNP is influenced by transported air masses from the Indian subcontinent, indicating that the concentration in Lhasa is high in the Tibetan Plateau. Compared to another typical highland site, Nyingchi, Lhasa, had much high levels of atmospheric Hg species, which may be related to the vegetation uptake effects and strong wet deposition in Nyingchi (Lin et al., 2022). Among the surrounding stations, only Mt. Gongga and Shangri-La stations had higher GEM concentrations than Lhasa. The GEM concentrations reported at Mt. Gongga station ranged from May 2005 to July 2006. Considering that the smelting activities near this site were crude at that time and there were almost no air pollution control measures, the high local GEM concentrations may be strongly affected by local smelting activities and fuel combustion (Fu et al., 2008). In contrast, GEM concentrations in the Shangri-La region were mainly controlled by the monsoon, and H. Zhang et al. (2015) suggested that all local GEM above 2.5 ng m^{-3} is associated with the transport of dry air carrying domestic and foreign regional anthropogenic emissions. Comparing these sites only for the monsoon period, the GEM concentration in Lhasa was higher than that in the Shangri-La region. As for GOM and PBM, the concentrations at the Lhasa station were much higher than those in the surrounding areas. The average GOM concentration in the surrounding areas was approximately 10 pg m^{-3}, which was only 27 % of that in Lhasa, and the average PBM concentration in the surrounding areas was approximately 28 pg m^{-3}, which was only 54 % of that in Lhasa. Considering that GOM and PBM are mainly from local or surrounding sources or atmospheric transport (Seigneur et al., 2006; Lynam et al., 2014; Lindberg and Stratton, 1998), high GOM and PBM concentrations may indicate additional local sources of Hg in Lhasa.

3.2 Unexpected high-concentration events in Lhasa

To investigate the reasons for the random events with high atmospheric Hg concentration in Lhasa, typical high-value occurrence processes (defined as GEM concentrations above

Table 1. Statistics metrics of species Hg, meteorological factors, and other pollutants.

Period	Stat	GEM ($ng\,m^{-3}$)	PBM ($pg\,m^{-3}$)	GOM ($pg\,m^{-3}$)	Temp (°C)	Hum. (%)	Wind speed ($m\,s^{-1}$)	Solar radiation ($W\,m^{-2}$)	CO ($mg\,m^{-3}$)	NO_2 ($\mu g\,m^{-3}$)	O_3 ($\mu g\,m^{-3}$)	$PM_{2.5}$ ($\mu g\,m^{-3}$)	SO_2 ($\mu g\,m^{-3}$)
S-ISM	Mean	2.73	59.08	38.39	14.42	61.45	1.70	212.60	0.39	26.44	72.18	16.26	4.19
	SD	1.48	181.38	62.85	3.70	16.96	1.41	313.90	0.18	19.36	28.68	13.12	2.08
	Median	2.36	24.50	30.30	13.90	62.00	1.30	7.00	0.30	22.00	77.00	13.00	4.00
	Min	0.40	−11.44	1.89	5.90	14.00	0.00	0.00	0.10	1.00	1.00	1.00	1.00
	Max	18.87	2165.70	988.50	24.70	93.00	13.00	1290.00	1.70	110.00	133.00	81.00	21.00
WEC1	Mean	2.39	57.55	37.46	6.90	26.01	1.28	169.56	0.64	45.24	45.39	47.97	5.51
	SD	2.35	104.15	50.98	5.75	15.08	1.39	246.66	0.51	31.01	34.44	46.19	5.35
	Median	1.79	38.80	27.83	6.90	24.00	0.90	0.00	0.50	41.00	43.00	35.00	5.00
	Min	0.31	0.00	1.89	−6.20	1.00	0.00	0.00	0.10	2.00	1.00	1.00	1.00
	Max	48.93	1797.30	774.86	21.60	94.00	9.80	973.00	4.40	152.00	133.00	458.00	145.00
WEC2	Mean	1.47	42.82	32.05	0.22	25.59	1.97	123.61	0.56	26.78	65.22	23.73	4.49
	SD	1.12	45.39	17.14	3.98	14.67	1.85	186.98	0.30	22.61	26.30	18.77	2.61
	Median	1.17	33.77	27.50	0.20	24.00	1.30	0.00	0.50	19.00	71.00	19.00	4.00
	Min	0.33	0.00	9.91	−8.80	2.00	0.00	0.00	0.20	2.00	1.00	1.00	1.00
	Max	20.86	589.43	165.06	10.20	68.00	11.20	662.00	2.60	99.00	108.00	118.00	32.00

$10\,ng\,m^{-3}$ monitored more than five times on a single day) were selected for analysis in the S-ISM and WEC periods, respectively. A total of seven events with high GEM concentration were identified, of which 3 September, 10 November, 19 November, and 9 December 2016 were selected for analysis, and 18 September 2016, 3 October 2016, and 27 January 2017 were omitted due to lack of meteorological data or Hg concentration data for the proximity date.

During the S-ISM period (Fig. 2), there was a clear peak in Hg concentration on 3 September, while the GEM, GOM, and PBM concentrations were approximately 1.6, 1.5, and 2.3 times the average daily value, respectively. Comparing the 2 d before and after the high-concentration event (Table 3, Fig. 3a), the concentrations of the three pollutants NO_2, $PM_{2.5}$, and SO_2 were higher on 3 September. High GEM concentrations were accompanied by winds of $2.12\,m\,s^{-1}$ from the southwest, with NO_2 and SO_2 concentrations higher than usual as well as increased PBM concentrations. NO_2 and SO_2 are typical combustion source pollutants, and the presence of $PM_{2.5}$ and PBM may indicate more combustion sources in the day. Thus, it can be inferred that the event with elevated Hg concentration on 3 September may have originated mainly from a combustion event nearby or further away.

During the WEC period, significantly high values were observed on 10 November, 19 November, and 9 December. On 10 November (Fig. 3b), the increase in atmospheric Hg species concentrations was accompanied by significant increases in CO, NO_2, PM_{10}, $PM_{2.5}$, and SO_2 concentrations. Two similar peaks in atmospheric Hg species concentrations were also observed around 10 November, with relatively lower peak concentrations. During these three events, the concentrations of other pollutants were higher than usual, whereas wind speeds were extremely low during the event periods. In addition, extremely high PBM concentrations ($297.7 \pm 189.3\,pg\,m^{-3}$, maximum $621.2\,pg\,m^{-3}$) were observed at midnight on 12 November, which, considering the extremely low wind speed and the presence of a low height nocturnal boundary layer, may indicate that the high concentrations originated from local sources.

On 19 November (Fig. 3c), there was a significant increase in all atmospheric Hg species concentrations. During the elevated period, the average GEM, GOM, and PBM concentrations were $17.94 \pm 10.54\,ng\,m^{-3}$, $302.5 \pm 218.5\,pg\,m^{-3}$, and $162.4 \pm 54.0\,pg\,m^{-3}$, respectively, which were 8.3, 5.7, and 4.6 times higher than the average concentrations on 17–18 November. However, only a slight increase in the peak CO, $PM_{2.5}$, and SO_2 concentration was observed during the event period. Therefore, the increase in atmospheric Hg species concentrations may indicate that this event was unique, with certain sources of high Hg concentrations. The low wind speed and low nocturnal boundary layer height both contributed to the accumulation of atmospheric Hg species, which also indicated that the elevated Hg was from local sources. Similar to the event on 19 November, sharp increases in atmospheric Hg species concentrations were only observed on 9 December (Fig. 3d). The atmospheric Hg species concentration increase events during the WEC period occurred at night, and, given that it coincided with the winter heating period, local combustion sources may be the unique sources that may contribute to the Hg concentration increase.

3.3 Diurnal variation of atmospheric Hg in Lhasa

Figure 4a shows the diurnal variation of atmospheric Hg in Lhasa during the monitoring period. The mean GEM concentration during this period was $2.26 \pm 1.97\,ng\,m^{-3}$, and the maximum difference of hourly average GEM diurnal variation was $1.89\,ng\,m^{-3}$. GEM concentration was low dur-

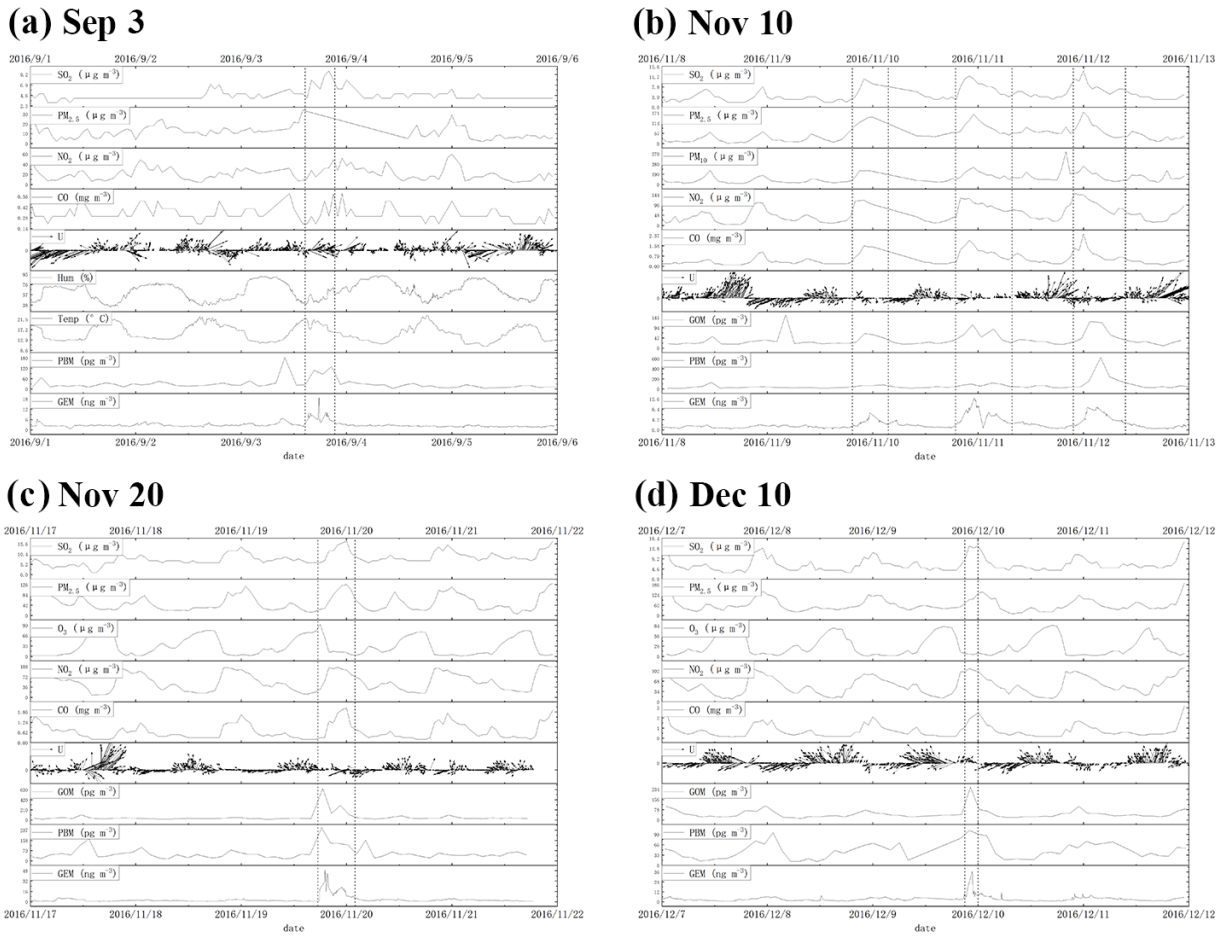

Figure 3. Comparison of the pollutant concentrations with those 2 d before and after the events with high Hg concentration. The dotted lines indicate the area where the Hg concentrations are significantly elevated.

ing the day; the lowest concentration of the day appeared from 14:00–18:00 (UTC+8). The GEM concentration kept increasing and reached a peak at midnight. During the night, the GEM concentration maintained in high value with little dissipation. Subsequently, the GEM concentration decreased rapidly with the sunrise. Overall, the diurnal variation of GEM concentration was similar to CO, NO_2, and relative humidity and opposite to O_3 and wind speed. The high GEM concentrations at night can be attributed to the lower boundary layer height at night (average at 131 m a.g.l., above ground level, during the observation period, between 19:00 and 07:00, UTC+8) and the lower wind speed (Fig. 4). Also, the average night temperature in Lhasa during the monitoring period was 5.8 °C, and the combustion from residents' use of heating may bring about the release of GEM. After sunrise, the boundary layer height increased rapidly, and the diffusion quickly occurred in the lower atmosphere. During the increase of wind speed, airflows were carried from other regions with low populations, which may lead to a decrease in GEM concentrations. For both GOM and PBM, the higher GOM concentrations occurred during the day, and higher PBM concentration occurred during the night. No obvious increase occurred for GOM and PBM concentrations at the same time, which may indicate that there is no local common external source, and the variation of GOM and PBM concentrations may come from the gas–particle redistribution process of atmospheric Hg(II).

In particular, during the S-ISM period (Fig. 4b), the diurnal variation in GEM concentrations fluctuated frequently, which indicates that the factors affecting the concentration variation were very complicated. The mean concentration of GEM during this period was 2.73 ng m^{-3}, and the maximum difference of GEM diurnal variation was 1.40 ng m^{-3}. September was the ending period of the Indian summer monsoon, and the external transboundary transport of air masses by the monsoon may have been weakened. Simultaneously, the average temperature in September was high (14.4 °C) without residents' use of heating during the night, which may be the reason for the small diurnal variation in GEM concentrations. Overall, GEM concentrations remained lower during the day, then increased, and remained high at night. No

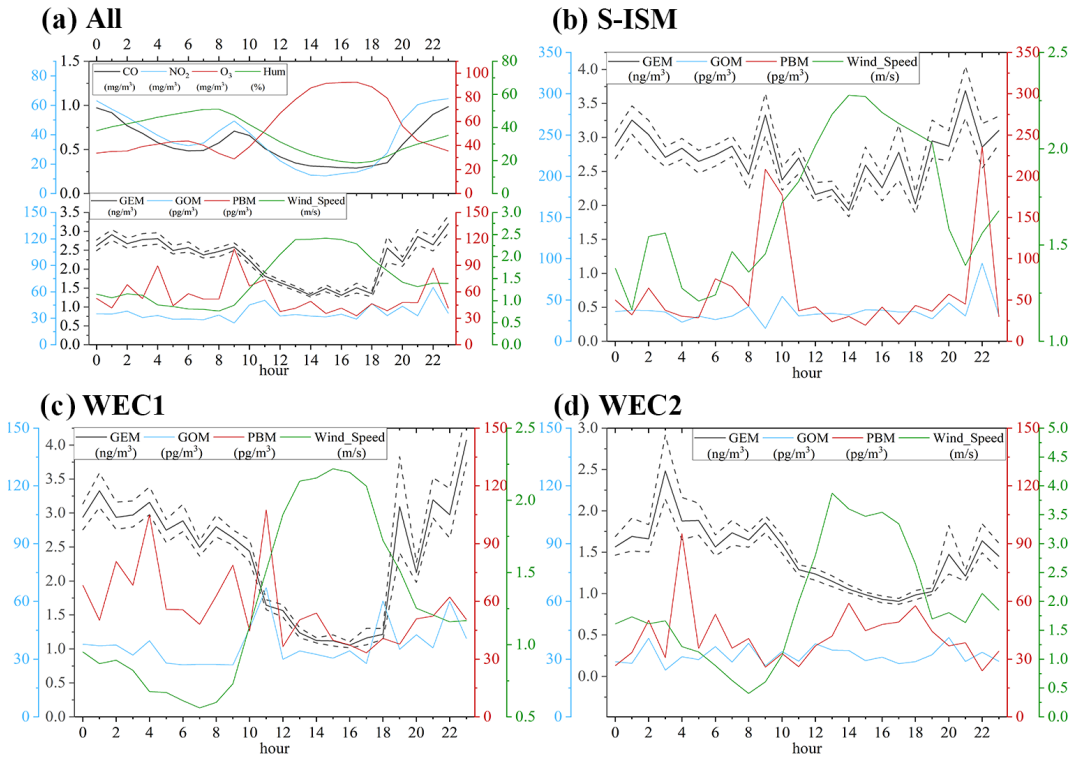

Figure 4. Diurnal variations of Hg species, concentrations of other pollutants, and meteorological information from S-ISM to WEC periods. The short horizontal line represents the concentration error range for each time period.

clear pattern of variation was observed in GOM and PBM during this period.

During the WEC1 period, the diurnal variation in GEM concentrations was exceedingly large. The mean GEM value was 2.39 ng m^{-3} with a large GEM diurnal variation value (3.01 ng m^{-3}). The diurnal trend was roughly the same as the whole monitoring period, but the lowest value was 1.06 ng m^{-3}, and the highest value was 4.07 ng m^{-3}. The increase in night concentrations may be related to the beginning of the heating season, whereas the burning of yak dung, firewood, or other fuels for residential heating may release GEM and PBM and accumulate within the boundary layer at night, leading to higher GEM concentrations (Rhode et al., 2007; Xiao et al., 2015; Chen et al., 2015). In contrast, low day values may be related to the wind field. Although the wind speed during the WEC1 period was similar to that during the S-ISM period, the westerly circulation was prevalent in Lhasa during the WEC1 period, with air masses coming from the sparsely populated area with lower GEM concentrations. The westerly winds carry away the locally accumulated GEM air masses in Lhasa and bring in low GEM concentration air masses from west of Lhasa. During this period, the diurnal variation in GOM concentrations was not clear.

The influence of wind flow was evident during the WEC2 period. During this period, GEM concentrations in Lhasa were the lowest and close to 1.00 ng m^{-3} in the late afternoon, when wind speeds were the highest. Nighttime concentrations were lower in the WEC2 period than in the WEC1 period, probably because wind speeds were also high at night during the WEC2 period (19:00–04:00 UTC+8, mean wind speed 1.74 m s^{-1}). The heating season was still in progress during the WEC2 period, but GEM emissions from heating were likely carried away by the continuous flow of air masses. Therefore, the mean GEM concentration in Lhasa during the winter was likely strongly influenced by wind speed.

Compared to the diurnal variation patterns obtained from monitoring in other remote areas of China (Fig. S3), the diurnal variation of GEM in Lhasa is more unique, and a wide diurnal variation in concentration was observed. Valleys of GEM concentrations in the afternoon were also observed in Waliguan and Namco, but the concentration variation ranges were small in both areas. This could be related to the regional characteristics of the three sites. Waliguan is located in a mountainous area with no significant local anthropogenic sources and is mainly influenced by valley winds (X. W. Fu et al., 2012). Namco is located in the central Tibetan region away from anthropogenic sources. Although the wind speed was also high in the afternoon in Namco (Yin et al., 2018), it is likely that the diurnal variation in atmospheric GEM concentrations was small because the atmosphere was well proportioned and there were no local sources; therefore, the

https://doi.org/10.5194/acp-23-3937-2023

Table 3. Comparison of the pollutant concentrations with the 2 d before and after the events with high Hg concentration. Note that data with large differences are highlighted in bold.

Item		1–2 Sep	**3 Sep**	4–5 Sep	8–9 Nov	**10 Nov**	11–12 Nov	17–18 Nov	**19 Nov**	20–21 Nov	7–8 Dec	**9 Dec**	10–11 Dec
GEM	($ng\,m^{-3}$)	2.72	**4.63**	3.03	1.47	**3.16**	**2.96**	2.15	**6.87**	2.66	2.76	**5.43**	3.24
PBM	($pg\,m^{-3}$)	25.32	**64.17**	31.52	36.31	**47.21**	**94.80**	53.41	**74.78**	55.40	38.71	**66.74**	49.05
GOM	($pg\,m^{-3}$)	40.95	**63.84**	42.55	32.76	**39.48**	**42.03**	35.29	**119.39**	44.86	43.84	**69.65**	43.75
Temp.	(°C)	16.61	15.86	15.32	7.06	7.76	8.80	4.20	4.49	4.94	3.13	2.88	2.77
Hum.	(%)	58.47	67.89	68.71	19.96	22.02	21.04	21.82	23.35	25.67	23.50	26.86	26.09
Wind speed	($m\,s^{-1}$)	2.37	1.46	1.49	1.47	**0.93**	1.17	1.05	**0.71**	0.75	0.88	0.89	0.67
Barometer	(hPa)	651.62	651.08	652.39	654.90	654.33	652.31	655.11	652.18	653.57	657.99	655.66	653.08
Rainfall	(mm)	0.01	0.17	0.36	0.00	0.00	0.00	0.00	0.00	0.00	0.00	0.00	0.00
Solar rad.	($W\,m^{-2}$)	241.20	201.15	214.39	189.02	194.45	182.30	166.14	161.59	180.02	141.61	139.69	136.64
CO	($mg\,m^{-3}$)	0.34	**0.36**	0.32	0.39	**0.76**	**0.63**	0.64	0.71	0.72	0.67	0.80	0.74
NO_2	($\mu g\,m^{-3}$)	20.44	**26.00**	21.77	41.38	**57.64**	**66.48**	54.58	53.58	55.27	48.87	55.33	56.23
O_3	($\mu g\,m^{-3}$)	85.73	77.42	72.56	59.27	57.43	49.46	34.73	34.79	29.51	31.37	28.38	26.81
PM_{10}	($\mu g\,m^{-3}$)	33.90	32.78	26.95	80.71	**130.07**	**155.44**	107.98	**119.79**	**146.29**	125.82	137.74	143.13
$PM_{2.5}$	($\mu g\,m^{-3}$)	11.98	**17.10**	10.98	31.20	**75.07**	**64.85**	51.21	50.13	53.83	62.80	65.46	62.71
SO_2	($\mu g\,m^{-3}$)	4.23	**5.89**	4.91	3.83	**6.07**	**5.71**	6.50	**8.92**	**9.44**	6.00	6.88	6.69

Table 2. Comparison of atmospheric Hg concentrations at some provincial capitals in China and some nearby monitoring stations.

Location	Altitude	Type	Region	Monitoring period	GEM	GOM	PBM	GEM diurnal variation (local time/GEM concentration)			Reference
					($ng\,m^{-3}$)	($pg\,m^{-3}$)	($pg\,m^{-3}$)	Peak ($ng\,m^{-3}$)	Valley ($ng\,m^{-3}$)	Variation ($ng\,m^{-3}$)	
Lhasa	3600	City	Southwest	Aug 2016–Feb 2017	2.26 ± 1.97	36.4 ± 48.9	54.5 ± 119.5				This study
Beijing	40	City	North China	Dec 2008–Nov 2009	3.22 ± 1.74	10.1 ± 18.8	98.2 ± 112.7				Zhang et al. (2013)
Hefei	30	City	East China	Jul 2013–Jun 2014	4.07 ± 1.91	3.67 ± 5.11	30.0 ± 100.3				Hong et al. (2016)
Shanghai	4	City	East China	2014	4.19 ± 9.13	21 ± 100	197 ± 877				Duan et al. (2017)
Lanzhou	1525	City	Northwest	Oct 2016–Oct 2017	4.48 ± 2.32						Yin et al. (2020)
Jinan	148	City	East China	Oct 2015–Jul 2016	4.91 ± 3.66		451.9 ± 433.4				Li et al. (2017)
Chongqing	300	City	Southwest	2006–2007	6.74 ± 0.37						Yang et al. (2009)
Nanjing	25	City	East China	2011	7.9 ± 7.0						Zhu et al. (2012)
Guiyang	1150	City	Southwest	Aug 2009–Dec 2009	9.72 ± 10.2	35.7 ± 43.9	368 ± 676				Liu et al. (2011)
Ev-K2, Nepal	5050	Remote		Nov 2011–Apr 2012	1.2 ± 0.2			18/1.30	6/1.10	0.20	Gratz et al. (2013)
Nam Co, China	5300	Remote		Nov 2014–Mar 2015	1.33 ± 0.24						Yin et al. (2018)
Waliguan, China	3816	Remote		Sep 2007–Sep 2008	1.98 ± 0.98	7.4 ± 4.8	19.4 ± 18.1	6/2.30	14/1.94	0.36	X. W. Fu et al. (2012)
Shangri-La, China	3580	Remote		Nov 2009–Nov 2010	2.51 ± 0.73	8.22 ± 7.9	38.32 ± 31.26	17/2.48	6/1.71	0.77	H. Zhang et al. (2015)
Gongga, China	1640	Remote		May 2005–Jun 2006	3.98			11/4.45	2/3.55	0.90	Fu et al. (2008)
QNNP, China	4267	Remote		Apr 2016–Aug 2016	1.42 ± 0.37	21.4 ± 13.4	25.6 ± 19.1	6/2.04	13/1.11	0.93	Lin et al. (2019)
Nyingchi, China	3263	Remote		Mar 2019–Sep 2019	1.01 ± 0.27	12.8 ± 13.3	9.3 ± 5.9	20/1.07	6/0.96	0.11	Lin et al. (2022)

changes in wind speed might not affect the GEM concentration. In contrast, with the difference in GEM concentrations between Lhasa and the transmitted external air mass, wind speed could significantly influence the GEM concentrations in Lhasa. Meteorological conditions may have played a more important role. We conjecture that the high nighttime concentrations in Lhasa may originate mainly from local emissions, while the high wind speed and mixing of clean external air masses in the afternoon reduce the local GEM concentrations.

3.4 Analysis of factors affecting atmospheric Hg concentration in Lhasa

Overall, four principal components were obtained for each period, from S-ISM to WEC2, using PCA, to analyze the relationships between Hg and multiple pollutants and meteorological variables. The Hg monitoring data, meteorological factors, and pollutant data in Lhasa were statistically and dimensionally reduced by PCA to analyze the relationships among them. The components related to Hg were selected and analyzed separately for each period, and the principal components were extracted (Table 4). According to the variable's loadings on each component, they were assigned the categories "special Hg-related factor", "local emission factor", and "wind factor".

A special Hg-related factor (Factor 1) was assigned owing to the continuous high positive loading of GEM, GOM, and PBM from the S-ISM to the WEC periods; only high positive loading of SO_2 was found in the WEC2 period. For this factor, there was no significant relationship with any other meteorological factors or pollutants. The high positive loading of this factor for all three Hg species and the low correlation with meteorological factors and other pollutants may indicate that this is a specific source of Hg. As the short transmission distance of the GOM and PBM, the special Hg-related source should be closer to Lhasa. However, no particular source of Hg around Lhasa has been reported in the literature, so the source indicated by this factor remains unclear.

Factor 2 had a slightly positive relationship with GEM and GOM; high positive loading of CO, NO_2, PM_{10}, $PM_{2.5}$, SO_2; and high negative loading of O_3 during the WEC period. The high positive loadings of CO, NO_2, PM_{10}, $PM_{2.5}$, and SO_2 may indicate that this factor is highly correlated with the combustion source. As O_3 concentration rapidly decreased after sunset (Fig. 4a), high negative loading of O_3 further indicated that this factor represented events during the nighttime with low O_3 concentrations. Since the WEC period overlapped with the heating season in Lhasa, Factor 2 may be strongly associated with heating combustion.

The wind factor (Factor 3) involves high positive loading of wind speed and low negative loading of GEM concentration during the S-ISM and WEC2 periods. This factor reveals the scavenging effect of wind on the local GEM in Lhasa. For high wind speed, the air masses with low GEM concentrations in the surrounding area mixed with the air masses in Lhasa, leading to a reduction in the GEM concentration. Concurrently, some GEM in Lhasa was carried away from the city by wind. At wind speeds greater than $4\,m\,s^{-1}$, the average GEM concentration in Lhasa was $1.31 \pm 0.93\,ng\,m^{-3}$, which is similar to the average concentration of Nam Co ($1.33 \pm 0.24\,ng\,m^{-3}$) in the Tibetan hinterland. Factor 3 was consistent with the analysis of the wind effect on the diurnal variation of Hg concentrations (Sect. 3.2), indicating the effect of strong winds on urban Hg removal.

3.5 Atmospheric Hg source trajectories and potential source regions in the Lhasa area

Figure 4 shows the GEM backward trajectory paths from the S-ISM period to the WEC2 period in Lhasa. During the S-ISM period, most trajectories (cluster 1, representative GEM concentration of $2.66\,ng\,m^{-3}$, 87.53 % of the trajectory during this period, Table S1 in the Supplement) originated from or passed through the south of Lhasa. The source of the trajectory points directly to the Indian Ocean, likely as these transported air masses are still subject to Indian monsoon action in September. According to the UNEP Hg emission inventory (UNEP, 2013), there are few anthropogenic emissions along this trajectory, indicating that the GEM may originate from the Indian Ocean or locally from Lhasa. Clusters 2 and 3 may indicate the trajectories of air masses driven by westerly circulation, which had a low proportion in the S-ISM period, with slightly different GEM concentrations from different sources.

During the WEC1 period, the driving factor of the air mass gradually shifted from Indian monsoon to westerly circulation. Clusters 2 and 3 are trajectories driven by the higher-height westerly circulation during the WEC1 period with a higher proportion than in the S-ISM period. Cluster 1 came from the southwest of Lhasa, and the air mass moved along the Himalayas before entering the Tibetan Plateau and was transported to Lhasa. Compared to the S-ISM period, the GEM concentration of this trajectory decreased slightly, which may be related to the source of the air mass and the areas it passes through. WEC2 showed little change in trajectory sources compared to WEC1, but all trajectory concentrations decreased significantly. Both WEC1 and WEC2 were in winter, and both had similar trajectories related to the driving wind field. Significantly decreasing GEM concentrations may suggest a local influence in the city of Lhasa. The local GEM in Lhasa consists of background concentrations superimposed on local emissions, and the share of local emissions decreases under better dispersion conditions (higher wind speeds) during the WEC2 period. The GEM concentration during the WEC2 period in Lhasa was only $0.16\,ng\,m^{-3}$ higher than that during the WEC period in the QNNP region ($1.31 \pm 0.42\,ng\,m^{-3}$; Lin et al., 2019).

Table 4. PCA factor loadings (varimax-rotated factor matrix) for Hg in Lhasa, China.

Tentative identification	Special Hg-related			Local emission		Wind	
Period	S-ISM	WEC1	WEC2	WEC1	WEC2	S-ISM	WEC2
GEM	**0.87**	**0.63**	**0.9**	0.44	0.3	−0.21	−0.13
PBM	**0.96**	**0.79**	**0.63**				
GOM	**0.95**	**0.87**	**0.95**	0.11	0.1		
Temp				−0.29	0.2		**0.92**
Hum		−0.19	0.17	−0.26	−0.18	−0.26	**−0.75**
Wind_Speed	−0.1	−0.14		−0.37		**0.87**	**0.91**
Rain							
Solar_Rad.				−0.21			
CO	0.17		0.11	**0.87**	**0.69**	−0.22	**0.51**
NO_2		0.13		**0.92**	**0.96**	−0.25	
O_3			−0.36	**−0.89**	**−0.83**	**0.53**	
PM_{10}	−0.14			**0.86**	**0.69**		0.14
$PM_{2.5}$	−0.16		0.16	**0.83**	**0.86**		
SO_2	0.26	0.17	**0.86**	**0.75**			
Variance explained	19.6	13.69	21.88	35.13	24.94	9.25	18.32

Note that variables with high factor loadings (> 0.5) are marked in bold. For readability, variables with very low factor loadings (< 0.1) are not presented.

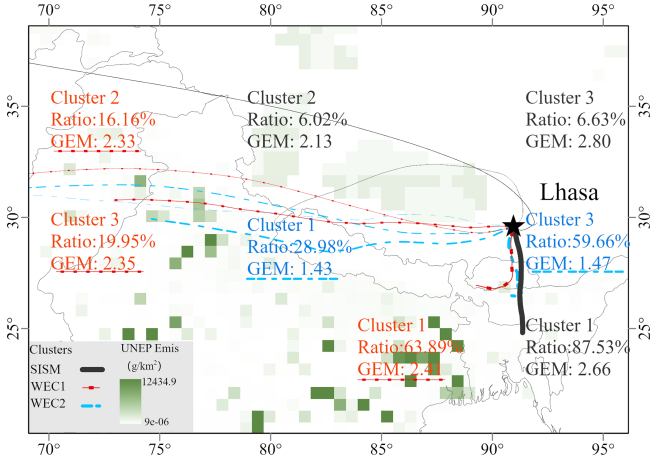

Figure 5. Clusters of the back trajectory analysis from Lhasa during S-ISM and WEC periods. The thickness of the line represents the ratio of the cluster in the time period, and the background is the global Hg emission inventory developed by UNEP (2013).

3.6 Comparison of three typical sites in the Tibetan Plateau

Different levels and variation patterns of Hg species concentrations were observed in the Qomolangma National Nature Preserve (QNNP; 4276 m) (Lin et al., 2019), Nyingchi (SET; 3263 m) (Lin et al., 2022), and Lhasa (3650 m) areas, which are typical monsoon-influenced, canyon, and urban areas in the Tibetan Plateau, respectively. Predictably, Hg species concentrations were generally lower in the Tibetan Plateau, while background areas with low populations in the plateau were lower than those on the plains in mainland China, and cities in the plateau were lower than those on the plains. Although the transboundary transport of pollutants has received considerable attention (Huang et al., 2016b; Wang et al., 2018; Lin et al., 2019; Zhu et al., 2019; Feng et al., 2019), the comparison between the QNNP and Lhasa indicates that the contribution of local anthropogenic sources may be significant for atmospheric pollutant concentrations. The comparison also suggests that atmospheric Hg emissions from urban residential life may be an important source that can be valuable in inventory studies.

Vastly different patterns of Hg species concentrations were found in the QNNP and SET due to differences in geography and vegetation cover. Atmospheric Hg transported to the QNNP is subject to a combination of monsoonal action and the pumping effect of glacial winds. However, atmospheric Hg entering the SET area has a slow elevation-increasing path, and abundant precipitation and vegetation have a significant trapping effect on atmospheric Hg. For Lhasa, a direct effect of local wind fields on the accumulation or rapid removal of GEM concentrations was found. This suggests that although global transport is important in the Hg cycle, the pollution at each location is likely to be strongly influenced by the local environment, even in exceptionally clean areas such as the Tibetan Plateau. However, there are still relatively few studies on GOM and PBM in the Tibetan Plateau, and more comprehensive investigations are required on how changes in Hg speciation transformation on snow and ice surfaces affect the environment, the effect of stratospheric intrusion on GOM concentrations (which is common in the plateau), and the effect of particulate matter on Hg(II) gas–

particle partitioning, which would help to understand the Hg species change in the plateau and throughout the world.

4 Conclusions

Lhasa is the largest city in the Tibetan Plateau; thus, its atmospheric Hg concentrations represent the highest level of atmospheric Hg pollution in this area. Unexpectedly high concentrations of atmospheric Hg species were found in Lhasa. The GEM concentrations were higher than the Northern Hemisphere background concentrations, and the GOM and PBM concentrations were high among Chinese cities. Monitoring of atmospheric Hg in Lhasa showed that the mean concentrations of GEM, GOM, and PBM during the S-ISM period ($2.73 \pm 1.48\,\mathrm{ng\,m^{-3}}$, $38.4 \pm 62.7\,\mathrm{pg\,m^{-3}}$, and $59.1 \pm 181.0\,\mathrm{pg\,m^{-3}}$, respectively) were higher than those during the WEC period ($2.11 \pm 2.09\,\mathrm{ng\,m^{-3}}$, $35.8 \pm 43.3\,\mathrm{pg\,m^{-3}}$, and $52.9 \pm 90.1\,\mathrm{pg\,m^{-3}}$, respectively). Combined with the trajectory analysis, the high atmospheric Hg concentrations during the S-ISM phase may have originated from external long-range transport.

Analysis of the overall concentration changes revealed some irregular and sudden events with high atmospheric Hg concentration in Lhasa. Analysis of these events suggests that local sources (such as combustion events) can cause events with severely elevated concentration under low wind speeds and the presence of a low-height nighttime boundary layer. Analysis of the diurnal variation of concentrations confirmed that low wind speeds and a low height nocturnal boundary layer would lead to the elevated local Hg concentrations. In contrast, higher wind speeds could rapidly remove atmospheric Hg from Lhasa. PCA of the influencing factors indicates that local sources, especially special Hg-related sources, are important factors influencing the variability of atmospheric Hg. The PCA also indicated the important role of higher wind speeds in reducing atmospheric Hg concentrations in the urban areas of Lhasa, likely owing to the large Hg concentration difference between Lhasa and surrounding areas.

Up to this study, we have obtained atmospheric Hg monitoring data from four typical areas of the Tibetan Plateau: Lhasa, the QNNP, SET, and Namco. The atmospheric Hg concentrations in the background areas were at or below the average GEM concentration of Northern Hemisphere, with higher levels in the urban area of Lhasa. Factors such as long-range transport of atmospheric Hg, effects of local meteorological conditions, and local glaciers were considered in these studies. Further monitoring of additional areas and regional simulations are required to confirm the atmospheric Hg transport patterns and fluxes.

Data availability. All the data presented in this paper can be made available for scientific purposes upon request to the corresponding authors.

Supplement. The supplement related to this article is available online at: https://doi.org/10.5194/acp-23-3937-2023-supplement.

Author contributions. HL, XW, YT, QiangZ, and XY designed the research and performed field measurements. HL and YT performed the data analysis and model simulations. HL led the paper writing. LC, CY, ZC, QianrZ, SK, JL, JS, and BdF contributed to the scientific discussion and the paper preparation.

Competing interests. The contact author has declared that none of the authors has any competing interests.

Disclaimer. Publisher's note: Copernicus Publications remains neutral with regard to jurisdictional claims in published maps and institutional affiliations.

Acknowledgements. This study was funded by the National Natural Science Foundation of China (grant nos. 41821005, 41977311, 42122059, and 41907328). The authors are grateful to NOAA for providing the HYSPLIT model and GFS meteorological files. We also thank the staff of Lhasa station of the Institute of Tibetan Plateau Research, Chinese Academy of Sciences, in Lhasa for field sampling assistance.

Financial support. This research has been supported by the National Natural Science Foundation of China (grant nos. 41821005, 41977311, 42122059, and 41907328).

Review statement. This paper was edited by Ralf Ebinghaus and reviewed by Yanxu Zhang and one anonymous referee.

References

Brooks, S., Luke, W., Cohen, M., Kelly, P., Lefer, B., and Rappenglück, B.: Mercury species measured atop the Moody Tower TRAMP site, Houston, Texas, Atmos. Environ., 44, 4045–4055, https://doi.org/10.1016/j.atmosenv.2009.02.009, 2010.

Chai, T., Crawford, A., Stunder, B., Pavolonis, M. J., Draxler, R., and Stein, A.: Improving volcanic ash predictions with the HYSPLIT dispersion model by assimilating MODIS satellite retrievals, Atmos. Chem. Phys., 17, 2865–2879, https://doi.org/10.5194/acp-17-2865-2017, 2017.

Chai, T., Stein, A., and Ngan, F.: Weak-constraint inverse modeling using HYSPLIT-4 Lagrangian dispersion model and Cross-Appalachian Tracer Experiment (CAPTEX) observations – effect of including model uncertainties on

source term estimation, Geosci. Model Dev., 11, 5135–5148, https://doi.org/10.5194/gmd-11-5135-2018, 2018.

Chen, P., Kang, S., Bai, J., Sillanpää, M., and Li, C.: Yak dung combustion aerosols in the Tibetan Plateau: Chemical characteristics and influence on the local atmospheric environment, Atmos. Res., 156, 58–66, https://doi.org/10.1016/j.atmosres.2015.01.001, 2015.

Cheng, I., Zhang, L., Blanchard, P., Graydon, J. A., and Louis, V. L. St.: Source-receptor relationships for speciated atmospheric mercury at the remote Experimental Lakes Area, northwestern Ontario, Canada, Atmos. Chem. Phys., 12, 1903–1922, https://doi.org/10.5194/acp-12-1903-2012, 2012.

Ci, Z., Zhang, X., Wang, Z., and Niu, Z.: Atmospheric gaseous elemental mercury (GEM) over a coastal/rural site downwind of East China: Temporal variation and long-range transport, Atmos. Environ., 45, 2480–2487, https://doi.org/10.1016/j.atmosenv.2011.02.043, 2011.

Cong, Z., Kang, S., Luo, C., Li, Q., Huang, J., Gao, S., and Li, X.: Trace elements and lead isotopic composition of PM_{10} in Lhasa, Tibet, Atmos. Environ., 45, 6210–6215, https://doi.org/10.1016/j.atmosenv.2011.07.060, 2011.

de Foy, B., Tong, Y., Yin, X., Zhang, W., Kang, S., Zhang, Q., Zhang, G., Wang, X., and Schauer, J. J.: First field-based atmospheric observation of the reduction of reactive mercury driven by sunlight, Atmos. Environ., 134, 27–39, https://doi.org/10.1016/j.atmosenv.2016.03.028, 2016.

Dommergue, A., Ferrari, C. P., Gauchard, P.-A., Boutron, C. F., Poissant, L., Pilote, M., Jitaru, P., and Adams, F. C.: The fate of mercury species in a sub-arctic snowpack during snowmelt, Geophys. Res. Lett., 30, 1621, https://doi.org/10.1029/2003gl017308, 2003.

Duan, L., Wang, X., Wang, D., Duan, Y., Cheng, N., and Xiu, G.: Atmospheric mercury speciation in Shanghai, China, Sci. Total Environ., 578, 460–468, https://doi.org/10.1016/j.scitotenv.2016.10.209, 2017.

Feng, X., Fu, X., and Zhang, H.: Observations of atmospheric Hg species and depositions in remote areas of China, E3S Web Conf., 1, 07001, https://doi.org/10.1051/e3sconf/20130107001, 2013.

Feng, Y., Wang, W., and Liu, J.: Dilemmas in and Pathways to Transboundary Water Cooperation between China and India on the Yaluzangbu-Brahmaputra River, Water, 11, 2096, https://doi.org/10.3390/w11102096, 2019.

Fu, X., Feng, X., Zhu, W., Wang, S., and Lu, J.: Total gaseous mercury concentrations in ambient air in the eastern slope of Mt. Gongga, South-Eastern fringe of the Tibetan plateau, China, Atmos. Environ., 42, 970–979, https://doi.org/10.1016/j.atmosenv.2007.10.018, 2008.

Fu, X., Feng, X., Sommar, J., and Wang, S.: A review of studies on atmospheric mercury in China, Sci. Total Environ., 421–422, 73–81, https://doi.org/10.1016/j.scitotenv.2011.09.089, 2012.

Fu, X., Zhu, W., Zhang, H., Sommar, J., Yu, B., Yang, X., Wang, X., Lin, C.-J., and Feng, X.: Depletion of atmospheric gaseous elemental mercury by plant uptake at Mt. Changbai, Northeast China, Atmos. Chem. Phys., 16, 12861–12873, https://doi.org/10.5194/acp-16-12861-2016, 2016.

Fu, X., Zhang, H., Feng, X., Tan, Q., Ming, L., Liu, C., and Zhang, L.: Domestic and Transboundary Sources of Atmospheric Particulate Bound Mercury in Remote Areas of China: Evidence from Mercury Isotopes, Environ. Sci. Technol., 53, 1947–1957, https://doi.org/10.1021/acs.est.8b06736, 2019.

Fu, X. W., Feng, X., Liang, P., Deliger, Zhang, H., Ji, J., and Liu, P.: Temporal trend and sources of speciated atmospheric mercury at Waliguan GAW station, Northwestern China, Atmos. Chem. Phys., 12, 1951–1964, https://doi.org/10.5194/acp-12-1951-2012, 2012.

Gay, D. A., Schmeltz, D., Prestbo, E., Olson, M., Sharac, T., and Tordon, R.: The Atmospheric Mercury Network: measurement and initial examination of an ongoing atmospheric mercury record across North America, Atmos. Chem. Phys., 13, 11339–11349, https://doi.org/10.5194/acp-13-11339-2013, 2013.

Gratz, L., Esposito, G., Dalla Torre, S., Cofone, F., Pirrone, N., and Sprovieri, F.: First Measurements of Ambient Total Gaseous Mercury (TGM) at the EvK2CNR Pyramid Observatory in Nepal, E3S Web Conf., 1, 27004, https://doi.org/10.1051/e3sconf/20130127004, 2013.

Guo, J., Kang, S., Huang, J., Zhang, Q., Tripathee, L., and Sillanpää, M.: Seasonal variations of trace elements in precipitation at the largest city in Tibet, Lhasa, Atmos. Res., 153, 87–97, https://doi.org/10.1016/j.atmosres.2014.07.030, 2015.

Hong, Q., Xie, Z., Liu, C., Wang, F., Xie, P., Kang, H., Xu, J., Wang, J., Wu, F., He, P., Mou, F., Fan, S., Dong, Y., Zhan, H., Yu, X., Chi, X., and Liu, J.: Speciated atmospheric mercury on haze and non-haze days in an inland city in China, Atmos. Chem. Phys., 16, 13807–13821, https://doi.org/10.5194/acp-16-13807-2016, 2016.

Horowitz, H. M., Jacob, D. J., Zhang, Y., Dibble, T. S., Slemr, F., Amos, H. M., Schmidt, J. A., Corbitt, E. S., Marais, E. A., and Sunderland, E. M.: A new mechanism for atmospheric mercury redox chemistry: implications for the global mercury budget, Atmos. Chem. Phys., 17, 6353–6371, https://doi.org/10.5194/acp-17-6353-2017, 2017.

Hu, Q. H., Kang, H., Li, Z., Wang, Y. S., Ye, P. P., Zhang, L. L., Yu, J., Yu, X. W., Sun, C., and Xie, Z. Q.: Characterization of atmospheric mercury at a suburban site of central China from wintertime to springtime, Atmos. Pollut. Res., 5, 769–778, https://doi.org/10.5094/apr.2014.086, 2014.

Huang, J., Kang, S., Shen, C., Cong, Z., Liu, K., Wang, W., and Liu, L.: Seasonal variations and sources of ambient fossil and biogenic-derived carbonaceous aerosols based on ^{14}C measurements in Lhasa, Tibet, Atmos. Res., 96, 553–559, https://doi.org/10.1016/j.atmosres.2010.01.003, 2010.

Huang, J., Kang, S., Wang, S., Wang, L., Zhang, Q., Guo, J., Wang, K., Zhang, G., and Tripathee, L.: Wet deposition of mercury at Lhasa, the capital city of Tibet, Sci. Total Environ., 447, 123–132, https://doi.org/10.1016/j.scitotenv.2013.01.003, 2013.

Huang, J., Kang, S., Guo, J., Zhang, Q., Cong, Z., Sillanpää, M., Zhang, G., Sun, S., and Tripathee, L.: Atmospheric particulate mercury in Lhasa city, Tibetan Plateau, Atmos. Environ., 142, 433–441, https://doi.org/10.1016/j.atmosenv.2016.08.021, 2016a.

Huang, J., Kang, S., Tian, L., Guo, J., Zhang, Q., Cong, Z., Sillanpää, M., Sun, S., and Tripathee, L.: Influence of long-range transboundary transport on atmospheric water vapor mercury collected at the largest city of Tibet, Sci. Total Environ., 566, 1215–1222, https://doi.org/10.1016/j.scitotenv.2016.05.177, 2016b.

Hurst, T. and Davis, C.: Forecasting volcanic ash deposition using HYSPLIT, J. Appl. Volcanol., 6, 5, https://doi.org/10.1186/s13617-017-0056-7, 2017.

Jackson, J. E.: A user's guide to principal components, John Wiley & Sons, ISBN 978-0-471-47134-9, 2005.

Jiskra, M., Sonke, J. E., Obrist, D., Bieser, J., Ebinghaus, R., Myhre, C. L., Pfaffhuber, K. A., Wängberg, I., Kyllönen, K., and Worthy, D.: A vegetation control on seasonal variations in global atmospheric mercury concentrations, Nat. Geosci., 11, 244–250, https://doi.org/10.1038/s41561-018-0078-8, 2018.

Kellerhals, M., Beauchamp, S., Belzer, W., Blanchard, P., Froude, F., Harvey, B., McDonald, K., Pilote, M., Poissant, L., Puckett, K., Schroeder, B., Steffen, A., and Tordon, R.: Temporal and spatial variability of total gaseous mercury in Canada: results from the Canadian Atmospheric Mercury Measurement Network (CAMNet), Atmos. Environ., 37, 1003–1011, https://doi.org/10.1016/s1352-2310(02)00917-2, 2003.

Lan, X., Talbot, R., Castro, M., Perry, K., and Luke, W.: Seasonal and diurnal variations of atmospheric mercury across the US determined from AMNet monitoring data, Atmos. Chem. Phys., 12, 10569–10582, https://doi.org/10.5194/acp-12-10569-2012, 2012.

Landis, M. S., Stevens, R. K., Schaedlich, F., and Prestbo, E. M.: Development and characterization of an annular denuder methodology for the measurement of divalent inorganic reactive gaseous mercury in ambient air, Environ. Sci. Technol., 36, 3000–3009, https://doi.org/10.1021/es015887t, 2002.

Li, C., Chen, P., Kang, S., Yan, F., Hu, Z., Qu, B., and Sillanpää, M.: Concentrations and light absorption characteristics of carbonaceous aerosol in $PM_{2.5}$ and PM_{10} of Lhasa city, the Tibetan Plateau, Atmos. Environ., 127, 340–346, https://doi.org/10.1016/j.atmosenv.2015.12.059, 2016a.

Li, C., Bosch, C., Kang, S., Andersson, A., Chen, P., Zhang, Q., Cong, Z., Chen, B., Qin, D., and Gustafsson, O.: Sources of black carbon to the Himalayan-Tibetan Plateau glaciers, Nat. Commun., 7, 12574, https://doi.org/10.1038/ncomms12574, 2016b.

Li, J., Lin, T., Qi, S., Zhang, G., Liu, X., and Li, K.: Evidence of local emission of organochlorine pesticides in the Tibetan plateau, Atmos. Environ., 42, 7397–7404, https://doi.org/10.1016/j.atmosenv.2008.06.030, 2008.

Li, Y., Wang, Y., Li, Y., Li, T., Mao, H., Talbot, R., Nie, X., Wu, C., Zhao, Y., Hou, C., Wang, G., Zhou, J., and Qie, G.: Characteristics and potential sources of atmospheric particulate mercury in Jinan, China, Sci. Total Environ., 574, 1424–1431, https://doi.org/10.1016/j.scitotenv.2016.08.069, 2017.

Lin, H., Tong, Y., Yin, X., Zhang, Q., Zhang, H., Zhang, H., Chen, L., Kang, S., Zhang, W., Schauer, J., de Foy, B., Bu, X., and Wang, X.: First measurement of atmospheric mercury species in Qomolangma Natural Nature Preserve, Tibetan Plateau, and evidence oftransboundary pollutant invasion, Atmos. Chem. Phys., 19, 1373–1391, https://doi.org/10.5194/acp-19-1373-2019, 2019.

Lin, H., Tong, Y., Yu, C., Chen, L., Yin, X., Zhang, Q., Kang, S., Luo, L., Schauer, J., de Foy, B., and Wang, X.: First observation of mercury species on an important water vapor channel in the southeastern Tibetan Plateau, Atmos. Chem. Phys., 22, 2651–2668, https://doi.org/10.5194/acp-22-2651-2022, 2022.

Lindberg, S., Bullock, R., Ebinghaus, R., Engstrom, D., Feng, X., Fitzgerald, W., Pirrone, N., Prestbo, E., Seigneur, C., and Panel on Source Attribution of Atmospheric Mercury: A synthesis of progress and uncertainties in attributing the sources of mercury in deposition, Ambio, 36, 19–32, https://doi.org/10.1579/0044-7447(2007)36[19:asopau]2.0.co;2, 2007.

Lindberg, S. E. and Stratton, W. J.: Atmospheric Mercury Speciation: Concentrations and Behavior of Reactive Gaseous Mercury in Ambient Air, Environ. Sci. Technol., 32, 49–57, https://doi.org/10.1021/es970546u, 1998.

Liu, B., Keeler, G. J., Dvonch, J. T., Barres, J. A., Lynam, M. M., Marsik, F. J., and Morgan, J. T.: Temporal variability of mercury speciation in urban air, Atmos. Environ., 41, 1911–1923, https://doi.org/10.1016/j.atmosenv.2006.10.063, 2007.

Liu, N., Qiu, G., Landis, M. S., Feng, X., Fu, X., and Shang, L.: Atmospheric mercury species measured in Guiyang, Guizhou province, southwest China, Atmos. Res., 100, 93–102, https://doi.org/10.1016/j.atmosres.2011.01.002, 2011.

Liu, S., Nadim, F., Perkins, C., Carley, R. J., Hoag, G. E., Lin, Y., and Chen, L.: Atmospheric mercury monitoring survey in Beijing, China, Chemosphere, 48, 97–107, https://doi.org/10.1016/s0045-6535(02)00026-7, 2002.

Lynam, M. M., Dvonch, J. T., Hall, N. L., Morishita, M., and Barres, J. A.: Spatial patterns in wet and dry deposition of atmospheric mercury and trace elements in central Illinois, USA, Environ. Sci. Pollut. R. International, 21, 4032–4043, https://doi.org/10.1007/s11356-013-2011-4, 2014.

Pant, N., Ravindra, R., Srivastava, D., and Thompson, L.: The Himalayan cryosphere: past and present variability of the "third pole", Geol. Soc. Lond. Spec. Publ., 462, SP462.413, https://doi.org/10.1144/SP462.13, 2018.

Pokhrel, B., Gong, P., Wang, X., Gao, S., Wang, C., and Yao, T.: Sources and environmental processes of polycyclic aromatic hydrocarbons and mercury along a southern slope of the Central Himalayas, Nepal, Environ. Sci. Pollut. Res. International, 23, 13843–13852, https://doi.org/10.1007/s11356-016-6443-5, 2016.

Qiu, J.: China: The third pole, Nature, 454, 393–396, https://doi.org/10.1038/454393a, 2008.

Rhode, D., Madsen, D. B., Brantingham, P. J., and Dargye, T.: Yaks, yak dung, and prehistoric human habitation of the Tibetan Plateau, Developments in Quaternary Sciences, 9, 205–224, https://doi.org/10.1016/S1571-0866(07)09013-6, 2007.

Rutter, A. P. and Schauer, J. J.: The impact of aerosol composition on the particle to gas partitioning of reactive mercury, Environ. Sci. Technol., 41, 3934–3939, https://doi.org/10.1021/es062439i, 2007.

Rutter, A. P., Schauer, J. J., Lough, G. C., Snyder, D. C., Kolb, C. J., Von Klooster, S., Rudolf, T., Manolopoulos, H., and Olson, M. L.: A comparison of speciated atmospheric mercury at an urban center and an upwind rural location, J. Environ. Monitor., 10, 102–108, https://doi.org/10.1039/b710247j, 2008.

Seigneur, C., Vijayaraghavan, K., and Lohman, K.: Atmospheric mercury chemistry: Sensitivity of global model simulations to chemical reactions, J. Geophys. Res., 111, D22306, https://doi.org/10.1029/2005jd006780, 2006.

Selin, N. E.: Global Biogeochemical Cycling of Mercury: A Review, Annu. Rev. Env. Resour., 34, 43–63, https://doi.org/10.1146/annurev.environ.051308.084314, 2009.

Slemr, F., Angot, H., Dommergue, A., Magand, O., Barret, M., Weigelt, A., Ebinghaus, R., Brunke, E.-G., Pfaffhuber, K. A., Ed-

wards, G., Howard, D., Powell, J., Keywood, M., and Wang, F.: Comparison of mercury concentrations measured at several sites in the Southern Hemisphere, Atmos. Chem. Phys., 15, 3125–3133, https://doi.org/10.5194/acp-15-3125-2015, 2015.

Song, S., Angot, H., Selin, N. E., Gallée, H., Sprovieri, F., Pirrone, N., Helmig, D., Savarino, J., Magand, O., and Dommergue, A.: Understanding mercury oxidation and air–snow exchange on the East Antarctic Plateau: a modeling study, Atmos. Chem. Phys., 18, 15825–15840, https://doi.org/10.5194/acp-18-15825-2018, 2018.

Sprovieri, F., Gratz, L., and Pirrone, N.: Development of a ground-based atmospheric monitoring network for the Global Mercury Observation System (GMOS), E3S Web Conf., 1, 17007, https://doi.org/10.1051/e3sconf/20130117007, 2013.

Sprovieri, F., Pirrone, N., Bencardino, M., D'Amore, F., Carbone, F., Cinnirella, S., Mannarino, V., Landis, M., Ebinghaus, R., Weigelt, A., Brunke, E.-G., Labuschagne, C., Martin, L., Munthe, J., Wängberg, I., Artaxo, P., Morais, F., Barbosa, H. D. M. J., Brito, J., Cairns, W., Barbante, C., Diéguez, M. D. C., Garcia, P. E., Dommergue, A., Angot, H., Magand, O., Skov, H., Horvat, M., Kotnik, J., Read, K. A., Neves, L. M., Gawlik, B. M., Sena, F., Mashyanov, N., Obolkin, V., Wip, D., Feng, X. B., Zhang, H., Fu, X., Ramachandran, R., Cossa, D., Knoery, J., Marusczak, N., Nerentorp, M., and Norstrom, C.: Atmospheric mercury concentrations observed at ground-based monitoring sites globally distributed in the framework of the GMOS network, Atmos. Chem. Phys., 16, 11915–11935, https://doi.org/10.5194/acp-16-11915-2016, 2016.

Steffen, A., Douglas, T., Amyot, M., Ariya, P., Aspmo, K., Berg, T., Bottenheim, J., Brooks, S., Cobbett, F., Dastoor, A., Dommergue, A., Ebinghaus, R., Ferrari, C., Gardfeldt, K., Goodsite, M. E., Lean, D., Poulain, A. J., Scherz, C., Skov, H., Sommar, J., and Temme, C.: A synthesis of atmospheric mercury depletion event chemistry in the atmosphere and snow, Atmos. Chem. Phys., 8, 1445–1482, https://doi.org/10.5194/acp-8-1445-2008, 2008.

Stein, A., Draxler, R. R., Rolph, G. D., Stunder, B. J., Cohen, M., and Ngan, F.: NOAA's HYSPLIT atmospheric transport and dispersion modeling system, B. Am. Meteorol. Soc., 96, 2059–2077, https://doi.org/10.1175/BAMS-D-14-00110.1, 2015.

Stylo, M., Alvarez, J., Dittkrist, J., and Jiao, H.: Global review of mercury monitoring networks, UNEP, Geneva, https://www.unep.org/resources/publication/global-review-mercury-monitoring-networks (last access: 30 March 2023), 2016.

Swartzendruber, P., Jaffe, D., and Finley, B.: Improved fluorescence peak integration in the Tekran 2537 for applications with sub-optimal sample loadings, Atmos. Environ., 43, 3648–3651, https://doi.org/10.1016/j.atmosenv.2009.02.063, 2009.

Tibet Bureau of Statistics (TBS): Tibet Statistics Yearbook, China Statistics Press, Beijing, ISBN 7503792124, 2020.

Travnikov, O., Angot, H., Artaxo, P., Bencardino, M., Bieser, J., D'Amore, F., Dastoor, A., De Simone, F., Diéguez, M. D. C., Dommergue, A., Ebinghaus, R., Feng, X. B., Gencarelli, C. N., Hedgecock, I. M., Magand, O., Martin, L., Matthias, V., Mashyanov, N., Pirrone, N., Ramachandran, R., Read, K. A., Ryjkov, A., Selin, N. E., Sena, F., Song, S., Sprovieri, F., Wip, D., Wängberg, I., and Yang, X.: Multi-model study of mercury dispersion in the atmosphere: atmospheric processes and model evaluation, Atmos. Chem. Phys., 17, 5271–5295, https://doi.org/10.5194/acp-17-5271-2017, 2017.

UNEP, Global Mercury Assessment: Sources, Emissions, Releases and Environmental Transport, UNEP Chemicals Branch, Switzerland, Geneva, 2013.

Venter, A. D., Beukes, J. P., van Zyl, P. G., Brunke, E.-G., Labuschagne, C., Slemr, F., Ebinghaus, R., and Kock, H.: Statistical exploration of gaseous elemental mercury (GEM) measured at Cape Point from 2007 to 2011, Atmos. Chem. Phys., 15, 10271–10280, https://doi.org/10.5194/acp-15-10271-2015, 2015.

Wang, C., Wang, X., Gong, P., and Yao, T.: Long-term trends of atmospheric organochlorine pollutants and polycyclic aromatic hydrocarbons over the southeastern Tibetan Plateau, Sci. Total Environ., 624, 241–249, https://doi.org/10.1016/j.scitotenv.2017.12.140, 2018.

Wang, X., Zhang, H., Lin, C. J., Fu, X., Zhang, Y., and Feng, X.: Transboundary transport and deposition of Hg emission from springtime biomass burning in the Indo-China Peninsula, J. Geophys. Res.-Atmos., 120, 9758–9771, https://doi.org/10.1002/2015jd023525, 2015.

Wang, X., Gong, P., Wang, C., Ren, J., and Yao, T.: A review of current knowledge and future prospects regarding persistent organic pollutants over the Tibetan Plateau, Sci. Total Environ., 573, 139–154, https://doi.org/10.1016/j.scitotenv.2016.08.107, 2016.

Xiao, Q., Saikawa, E., Yokelson, R. J., Chen, P., Li, C., and Kang, S.: Indoor air pollution from burning yak dung as a household fuel in Tibet, Atmos. Environ., 102, 406–412, https://doi.org/10.1016/j.atmosenv.2014.11.060, 2015.

Yang, J., Kang, S., Ji, Z., and Chen, D.: Modeling the Origin of Anthropogenic Black Carbon and Its Climatic Effect Over the Tibetan Plateau and Surrounding Regions, J. Geophys. Res.-Atmos., 123, 671–692, https://doi.org/10.1002/2017jd027282, 2018.

Yang, Y., Chen, H., and Wang, D.: Spatial and temporal distribution of gaseous elemental mercury in Chongqing, China, Environ. Monit. Assess., 156, 479–489, https://doi.org/10.1007/s10661-008-0499-8, 2009.

Yao, T., Thompson, L. G., Mosbrugger, V., Zhang, F., Ma, Y., Luo, T., Xu, B., Yang, X., Joswiak, D. R., Wang, W., Joswiak, M. E., Devkota, L. P., Tayal, S., Jilani, R., and Fayziev, R.: Third Pole Environment (TPE), Environmental Development, 3, 52–64, https://doi.org/10.1016/j.envdev.2012.04.002, 2012.

Yin, X., Kang, S., de Foy, B., Ma, Y., Tong, Y., Zhang, W., Wang, X., Zhang, G., and Zhang, Q.: Multi-year monitoring of atmospheric total gaseous mercury at a remote high-altitude site (Nam Co, 4730 m a.s.l.) in the inland Tibetan Plateau region, Atmos. Chem. Phys., 18, 10557–10574, https://doi.org/10.5194/acp-18-10557-2018, 2018.

Yin, X., Zhou, W., Kang, S., de Foy, B., Yu, Y., Xie, J., Sun, S., Wu, K., and Zhang, Q.: Latest observations of total gaseous mercury in a megacity (Lanzhou) in northwest China, Sci. Total Environ., 720, 137494, https://doi.org/10.1016/j.scitotenv.2020.137494, 2020.

Zhang, H., Fu, X. W., Lin, C.-J., Wang, X., and Feng, X. B.: Observation and analysis of speciated atmospheric mercury in Shangri-La, Tibetan Plateau, China, Atmos. Chem. Phys., 15, 653–665, https://doi.org/10.5194/acp-15-653-2015, 2015.

Zhang, H., Fu, X., Lin, C.-J., Shang, L., Zhang, Y., Feng, X., and Lin, C.: Monsoon-facilitated characteristics and transport of atmospheric mercury at a high-altitude background site in southwestern China, Atmos. Chem. Phys., 16, 13131–13148, https://doi.org/10.5194/acp-16-13131-2016, 2016.

Zhang, L., Wang, S. X., Wang, L., and Hao, J. M.: Atmospheric mercury concentration and chemical speciation at a rural site in Beijing, China: implications of mercury emission sources, Atmos. Chem. Phys., 13, 10505–10516, https://doi.org/10.5194/acp-13-10505-2013, 2013.

Zhang, R., Wang, H., Qian, Y., Rasch, P. J., Easter, R. C., Ma, P.-L., Singh, B., Huang, J., and Fu, Q.: Quantifying sources, transport, deposition, and radiative forcing of black carbon over the Himalayas and Tibetan Plateau, Atmos. Chem. Phys., 15, 6205–6223, https://doi.org/10.5194/acp-15-6205-2015, 2015.

Zhou, H., Hopke, P. K., Zhou, C., and Holsen, T. M.: Ambient mercury source identification at a New York State urban site: Rochester, NY, Sci. Total Environ., 650, 1327–1337, https://doi.org/10.1016/j.scitotenv.2018.09.040, 2019.

Zhu, J., Wang, T., Talbot, R., Mao, H., Hall, C. B., Yang, X., Fu, C., Zhuang, B., Li, S., Han, Y., and Huang, X.: Characteristics of atmospheric Total Gaseous Mercury (TGM) observed in urban Nanjing, China, Atmos. Chem. Phys., 12, 12103–12118, https://doi.org/10.5194/acp-12-12103-2012, 2012.

Zhu, J., Xia, X., Che, H., Wang, J., Cong, Z., Zhao, T., Kang, S., Zhang, X., Yu, X., and Zhang, Y.: Spatiotemporal variation of aerosol and potential long-range transport impact over the Tibetan Plateau, China, Atmos. Chem. Phys., 19, 14637–14656, https://doi.org/10.5194/acp-19-14637-2019, 2019.